ADVANCED FUNCTIONAL MATERIALS
www.afm-journal.de

Statistical Piezotronic Effect in Nanocrystal Bulk by Anisotropic Geometry Control

Shuhai Liu, Ming Han, Xiaolong Feng, Qiuhong Yu, Long Gu, Longfei Wang, Yong Qin,* and Zhong Lin Wang**

Utilizing inner-crystal piezoelectric polarization charges to control carrier transport across a metal-semiconductor or semiconductor–semiconductor interface, piezotronic effect has great potential applications in smart micro/nano-electromechanical system (MEMS/NEMS), human-machine interfacing, and nanorobotics. However, current research on piezotronics has mainly focused on systems with only one or rather limited interfaces. Here, the statistical piezotronic effect is reported in ZnO bulk composited of nanoplatelets, of which the strain/stress-induced piezo-potential at the crystals' interfaces can effectively gate the electrical transport of ZnO bulk. It is a statistical phenomenon of piezotronic modification of large numbers of interfaces, and the crystal orientation of inner ZnO nanoplatelets strongly influence the transport property of ZnO bulk. With optimum preferred orientation of ZnO nanoplatelets, the bulk exhibits an increased conductivity with decreasing stress at a high pressure range of 200–400 MPa, which has not been observed previously in bulk. A maximum sensitivity of 1.149 µS m^{-1} MPa^{-1} and a corresponding gauge factor of 467–589 have been achieved. As a statistical phenomenon of many piezotronic interfaces modulation, the proposed statistical piezotronic effect extends the connotation of piezotronics and promotes its practical applications in intelligent sensing.

1. Introduction

It is important to investigate the physics of interfacial phenomena in semiconductor devices[1] for their applications in electronics[2] and optoelectronics.[3] As the promising approaches for multifunctional electronics, utilizing local polarization produced by piezoelectric, ferroelectric or flexoelectric effects to modulate the interface bandstructure has attracted much attentions.[4] For example, coupling between the piezoelectricity (**Figure 1**a) and the semiconducting properties, piezotronics has been widely considered as an effective way for active electronics. It uses strain-induced piezoelectric charges at the interface to redistribute the free carriers and thus modify the energy profile, so as to tune the electronic transport at interface/junction.[5] The coupling effect of mechanical stimuli and carrier transport opens pathways to new designs of multifunctional devices with adaptive interaction between electronics and physical environment for applications including tunable electronics, human-machine interface, and artificial intelligence.[6]

By now, the researches about piezotronic effect mainly focus on the systems with only one or rather limited interfaces.[7] Few studies have been achieved on complex systems containing nanocrystals with large numbers of interfaces, as schematically illustrated in Figure 1b. Effective control of such systems is a big challenge, because of the complex and uncontrollable nanocrystal orientation and the corresponding piezo-potential distribution. The interface barriers formed between adjacent nanocrystals, increase, decrease or remain unmodified depending on the orientation of piezoelectric nanocrystals. Typically, there exists six kinds of interface regulations inside the system when under

Prof. S. Liu, M. Han, Q. Yu, Prof. L. Gu
School of Advanced Materials and Nanotechnology
Xidian University
Xi'an, Shaanxi 710071, China

Prof. S. Liu, Prof. Y. Qin
Institute of Nanoscience and Nanotechnology
School of Physical Science and Technology
Lanzhou University
Lanzhou, Gansu 730000, China
E-mail: qinyong@lzu.edu.cn

X. Feng
Research Laboratory for Quantum Materials
Singapore University of Technology and Design
Singapore 487372, Singapore

Dr. L. Wang, Prof. Z. L. Wang
Beijing Institute of Nanoenergy and Nanosystems
Chinese Academy of Sciences
Beijing 100083, China
E-mail: lfwang12@binn.cas.cn; zhong.wang@mse.gatech.edu

Dr. L. Wang, Prof. Z. L. Wang
College of Nanoscience and Technology
University of Chinese Academy of Sciences
Beijing 100049, China

Dr. L. Wang, Prof. Z. L. Wang
School of Material Science and Engineering
Georgia Institute of Technology
Atlanta, Georgia 30332, USA

The ORCID identification number(s) for the author(s) of this article can be found under https://doi.org/10.1002/adfm.202010339.

DOI: 10.1002/adfm.202010339

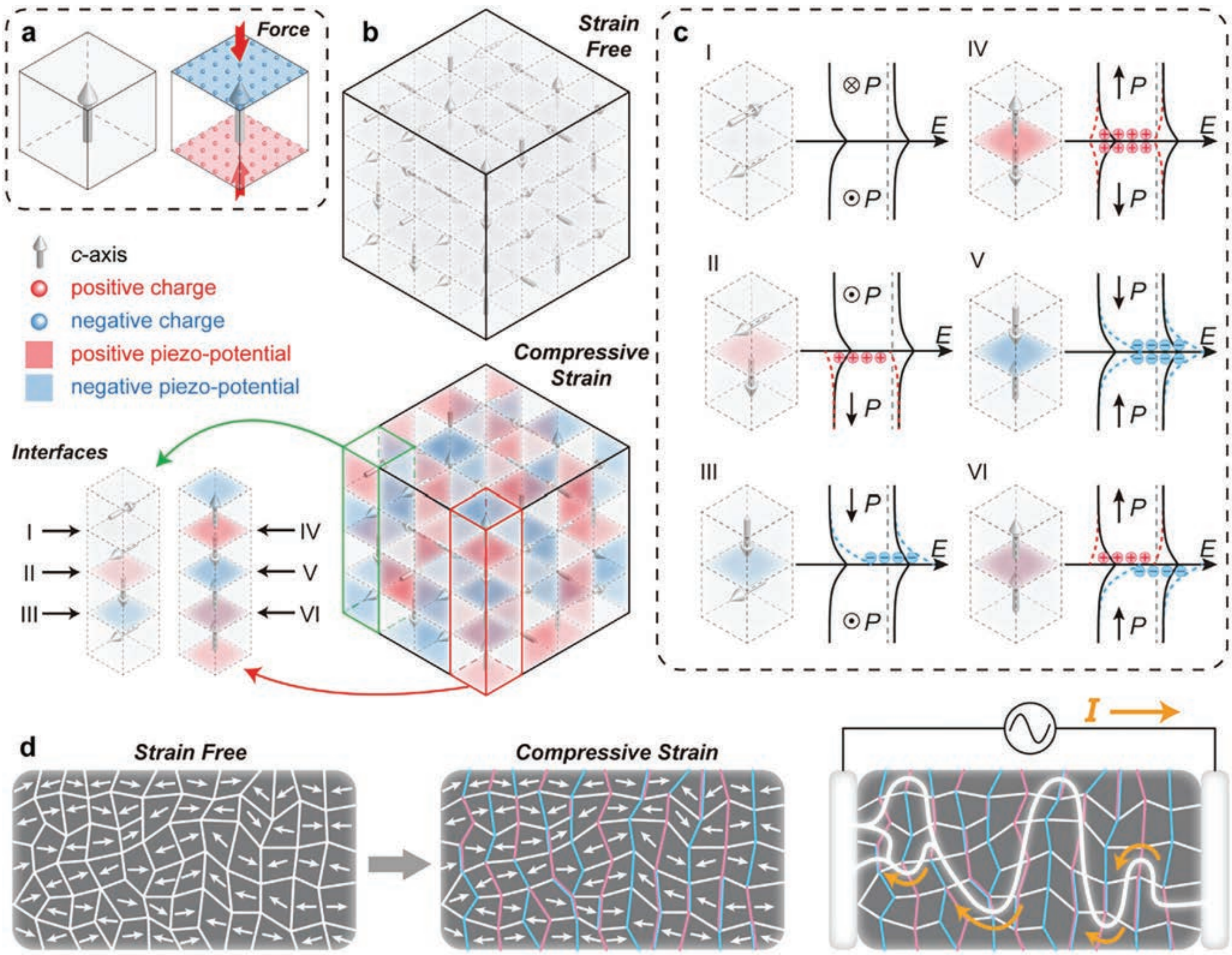

Figure 1. Illustration of statistical piezotronic effect. a) Piezoelectric effect. The polarization charges and piezoelectric potentials correspond to the *c*-axis of simplified piezoelectric unit under compressive strain. b) Piezoelectric potentials produced at large numbers of interfaces between piezoelectric crystals with strain free and compressive strain. c) Six typical piezotronic modifications of the interface energy structure. Double Schottky barrier remains unchanged (I, "side-to-side"), decreases at one side (II, "side-to-tail"), increases at one side (III "side-to-head"), decreases at both sides (IV, "tail-to-tail"), increases at both sides (V, "head-to-head"), or increases at one side but decreases at another side (VI, "tail-to-head"). Note: case (IV) and (V) respectively correspond to the interface electrical conduction ("ON" state) and electrical obstruction ("OFF" state). d) Schematic diagram of a bulk containing large numbers of *c*-axis preferred piezoelectric units with strain free and compressive strain, and the corresponding current channel controlled by the statistical piezotronic modification of large numbers of interfaces. The solid white line and arrow indicate interface and piezoelectric polarization (*c*-axis), respectively. The solid red and blue lines represent positive and negative piezoelectric potentials generated at interfaces, respectively. The white glow line represents the current channel across the bulk. Note: under the illustrated piezoelectric potential distribution, the current channel twists and turns, leading to a high-resistance state of the bulk.

compressive stress (Figure 1c), including double Schottky barrier unchanged (I, "side-to-side"), decreased at one side (II, "side-to-tail"), increased at one side (III "side-to-head"), decreased at both sides (IV, "tail-to-tail"), increased at both sides (V, "head-to-head") and increased at one side and decreased at another side (VI, "tail-to-head"). Due to the uncontrollable nanocrystal orientation, such system is generally regulated by randomly distributed piezo-potential and exhibits an immutable electrical behavior with applied uniaxial compressive stress,[8] which greatly hinders the practical applications of piezotronic effect in multi-component systems. Therefore, it is highly desired to explore a feasible and controllable approach that can realize and utilize the piezotronic modification of large numbers of interfaces in bulks.

In this work, a statistical piezotronic effect is proposed for the regulation of ZnO bulk made of ZnO nanoplatelets with preferred orientations. It utilizes the statistical distribution of crystal orientation and the corresponding piezo-potential at the crystals' interfaces under compressive stress to control the electrical transport of ZnO bulk. Compared with the bulk made of randomly oriented ZnO nanoparticles, the one with *c*-axis preferred ZnO nanoplatelets exhibits an increased conductivity with decreasing stress at high pressure range of 200–400 MPa, which has not been observed previously in bulk. The bulk with optimum preferred crystal orientation of ZnO nanoplatelets realizes a maximum sensitivity of 1.149 μS m^{-1} MPa^{-1} and a corresponding gauge factor of 467–589. Unlike the regulation for limited numbers of interfaces, the statistical piezotronic effect proposed here is performed at large numbers of interfaces, which will open up the macroscopic practical applications of piezotronics in intelligent sensing and will greatly increase the sensitivity of traditional force sensors or strain sensors.

2. Results and Discussion

2.1. Principle of Statistical Piezotronic Effect

The basic principle of statistical piezotronic effect is schematically illustrated in Figure 1d. The bulk with optimum preferred orientation of ZnO nanocrystals under uniaxial compressive stress will result in piezo-potentials along a certain direction. Positive (red) and negative (blue) piezo-potentials can respectively decrease and increase the interface barriers. The barrier height increases, decreases or remains unmodified at interfaces respectively labeled as blue, red and white lines, depending on the crystal orientations of adjacent nanocrystals. Electrons can flow through the interfaces with decreased barriers (red lines) or with little resistance, while require higher energy to pass through the ones with increased barriers (blue lines). Large numbers of individual nanoscale interfaces modulated by oriented piezopotential will eventually lead current channel winding and zigzag (particularly labeled with white glow line) and require electrons to go a longer distance from one end of the bulk to the other end. In this way, the bulk with optimum preferred orientation of ZnO nanocrystals will exhibit a deceased conductivity with increasing pressure. A more detailed 2D illustration is presented in Note S1 and Figure S1 (Supporting Information).

2.2. Electrical Property of the Bulk Made of ZnO Spherical Nanoparticles under Pressures

In order to verify this scheme and characterize the electrical transport of bulks under different pressures, the equipment was set up as illustrated in **Figure 2**a. It mainly consists of two parts: one is a hydraulic jack, which is mainly used to offer a high uniaxial pressure (0–500 MPa); the other is an electrical measurement system, used to apply a voltage across the bulk and simultaneously measure their electrical transport.

Using this equipment, we first studied the bulk consisting of ZnO spherical nanoparticles (Note S2 and Figure S2, Supporting Information) with randomly oriented polar *c*-axis, as shown in Figure 2b. At the beginning, the powder of ZnO spherical nanoparticles was filled into the jack mold, and then, was pressed into a bulk by gradually increasing the uniaxial pressure to a very high value of about 500 MPa. This pressure was remained roughly constant for about 12 h to get a ZnO nanoparticle bulk with stable structure. Second, after decreasing the applied pressure to a preset value, the pressure remained constant and the electrical measurements were made. At this stage, a sweeping bias between −1 and +1 V was applied and the current was measured simultaneously. After the *I*–*V* measurements were performed, the pressure was adjusted to the next preset value to start measuring the electrical characteristics under this new set pressure.

Prior to the *I*–*V* measurements, the nanoparticle's crystal orientation in pressed ZnO bulk was characterized. Since the ZnO nanoparticles are approximately spherical and hence have no shape anisotropy related to the crystal orientation, the nanoparticles in bulks will not exhibit preferred orientation, but remain randomly oriented, which can be seen from the X-ray diffraction spectra before and after compressing (Figure S3, Supporting Information). Also, by calculating the Lotgering orientation factor f [9] (Note S3 and Table S1, Supporting Information), the orientation degree of ZnO spherical nanoparticles in the form of powder before compression and bulk after compression can be evaluated from the XRD data. Compared with the standard random sample (PDF#36-1451), no preferred orientation and almost a same random orientation distribution were found both in the powder and the bulks (Figure S3, Supporting Information), which confirms the random distribution of the crystal orientation of ZnO spherical nanoparticles in bulks.

In the subsequent *I*–*V* measurements, a pressure ranged from 30.4 to 480.1 MPa was applied to ZnO bulk composed of ZnO spherical nanoparticles. As shown in Figure 2c,d, an enhanced conductivity can be found when applied uniaxial compressive stresses. Being subjected to external stimuli, ZnO spherical nanoparticles in the bulk will experience compressive strains and produce piezoelectric charges across each two ends, which distributed within a thickness of 1–2 atomic layers.[10] The charge distribution around the interface can be modeled as a combination of a trapped negative interface charges, two positive depletion layers, and two piezoelectric polarization charges. The sign of piezoelectric charges depends on the polarization *c*-axis of adjacent nanoparticles. Due to the randomly crystal's orientation of spherical nanoparticles, the distribution of piezoelectric charges and potentials inside the bulk belong to a random one. Therefore, the conductivity of such ZnO bulk composed of ZnO spherical nanoparticles increases as the pressure increases, which is mainly attributed to the piezoelectric effect between randomly oriented nanoparticles. It is consistent with previous reports.[8b,11]

The electron affinity of ZnO and the work function of electrodes (Fe) are both ≈4.5 eV,[12] resulting in a little barrier at the ZnO-Fe interface and an Ohmic contact. The electrical characteristics show a symmetric property under both forward bias and reverse bias, whereas the *I*–*P* curve derived from the *I*–*V* curves is asymmetric (Figure 2d). That is, under small pressures, the positive-biased and the negative-biased currents are slightly different from each other. It may result from the unevenness of the stress across the bulk caused by the pressure transmission among the nanoparticles.

Additionally, the same measurements were also performed on the ZnO spherical nanoparticles bulk after it was sintered, as shown in Figure 2e,f. The current increases gradually with increasing pressure, which is same as the one without sintering. The difference is that the forward and reverse currents here overlap very well, indicating a symmetric carrier transport of the sintered bulk. By plotting the current presented in semilog form via applied pressure, it is found to be in good agreement with previous theory prediction in ZnO varistor[8b] (Note S4 and Figure S4, Supporting Information). It shows that the sintered bulk composed of randomly oriented ZnO spherical nanoparticles exhibits the same *I*–*P* characteristics as a

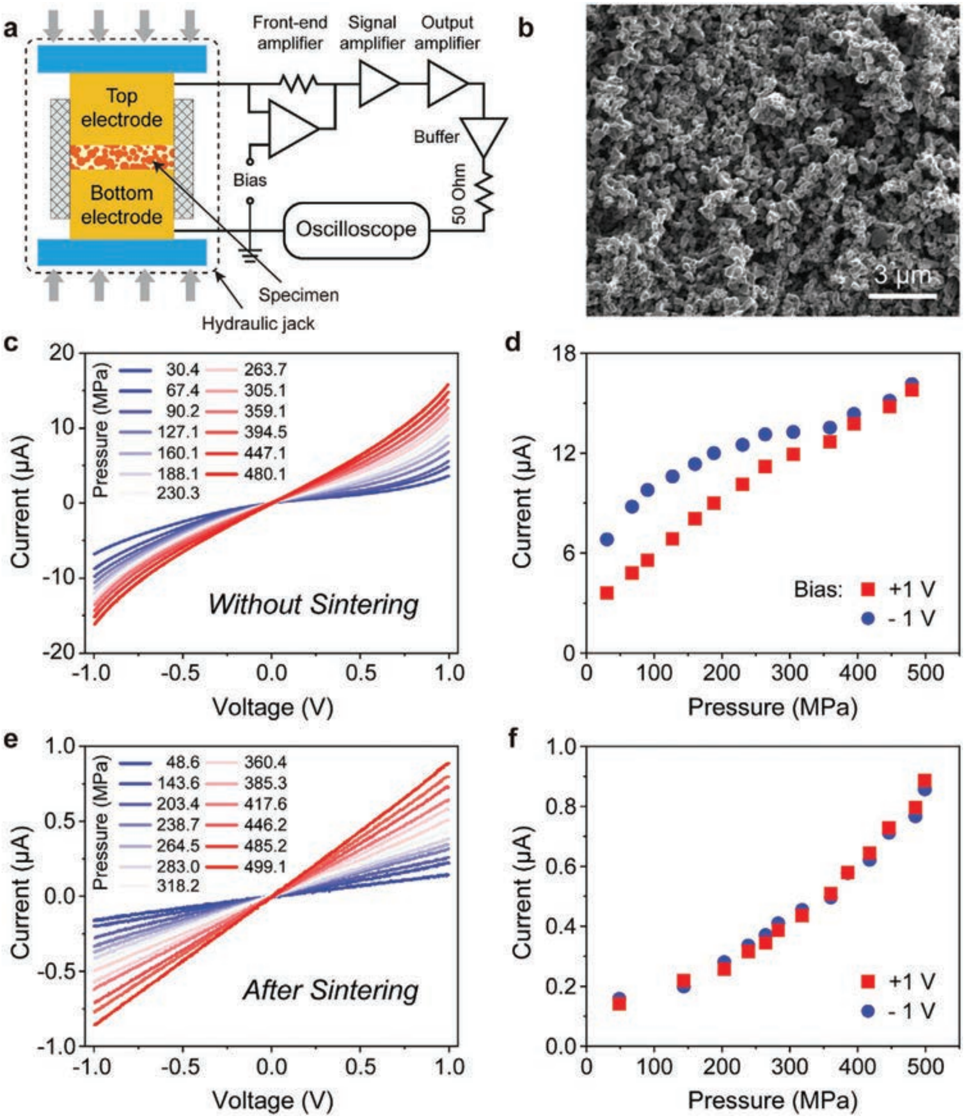

Figure 2. Electrical properties of the bulk made of ZnO spherical nanoparticles as a function of mechanical pressure. a) Schematic diagram of the measurement setup. The electrical transport is performed under different pressures. b) SEM image of ZnO nanoparticles, which has no shape feature related to the crystal orientation and is approximately spherical. c) *I–V* and d) *I–P* characteristics of the ZnO bulk composed of ZnO spherical nanoparticles without sintering under a pressure ranged from 30.4 to 480.1 MPa, indicating an enhanced current with increased pressure. e) *I–V* and f) *I–P* characteristics of the same ZnO bulk in (c,d) after sintering under a pressure ranged from 48.6 to 499.1 MPa. An increased current is also shown with increased pressure.

varistor. It is also worth noting here that, compared with the one without sintering, the sintered ZnO bulk demonstrates a lower current under the same bias voltage, which may result from the enhanced crystallinity and the reduced conductivity through sintering.

2.3. Theoretical Simulation of Statistical Piezotronic Effect

The commonly used "Finite Element Analysis" (FEA) shows limited performance in bulks composed of huge numbers of nanocrystals with lots of interfaces. So, an equivalent circuit model is built here to analyze bulks with millions of nanocrystal units (**Figure 3**a). Each piezoelectric nanocrystal is simplified as a cube with six surfaces, and is equivalent to a circuit cell consisting of six diodes. Contact potential between adjacent nanocrystals is also considered as a strain-controlled resistance ($R \propto \varepsilon^{-k}$, $0.5 < k < 1.0$, Note S5 and Figures S5 and S6, Supporting Information).[13] Information about the equivalent circuit cell model has been detailed in Note S6 and Figure S7 (Supporting Information). In Figure 3b, by properly adjusting the parameters (e.g., threshold voltage) of the corresponding equivalent circuit cell (including the diodes and strain-controlled resistance), we can approximate the strain-controlled *I–V* curves of typical interfaces "IV," "V," and "VI" in Figure 1c, which is in well agreement with the result simulated by the method of FEA. It indicates the feasibility of using equivalent circuit cell to simplify the piezoelectric nanocrystal, which greatly reduces the computational complexity. Using this simplification, we can equate a bulk with millions of nanocrystals

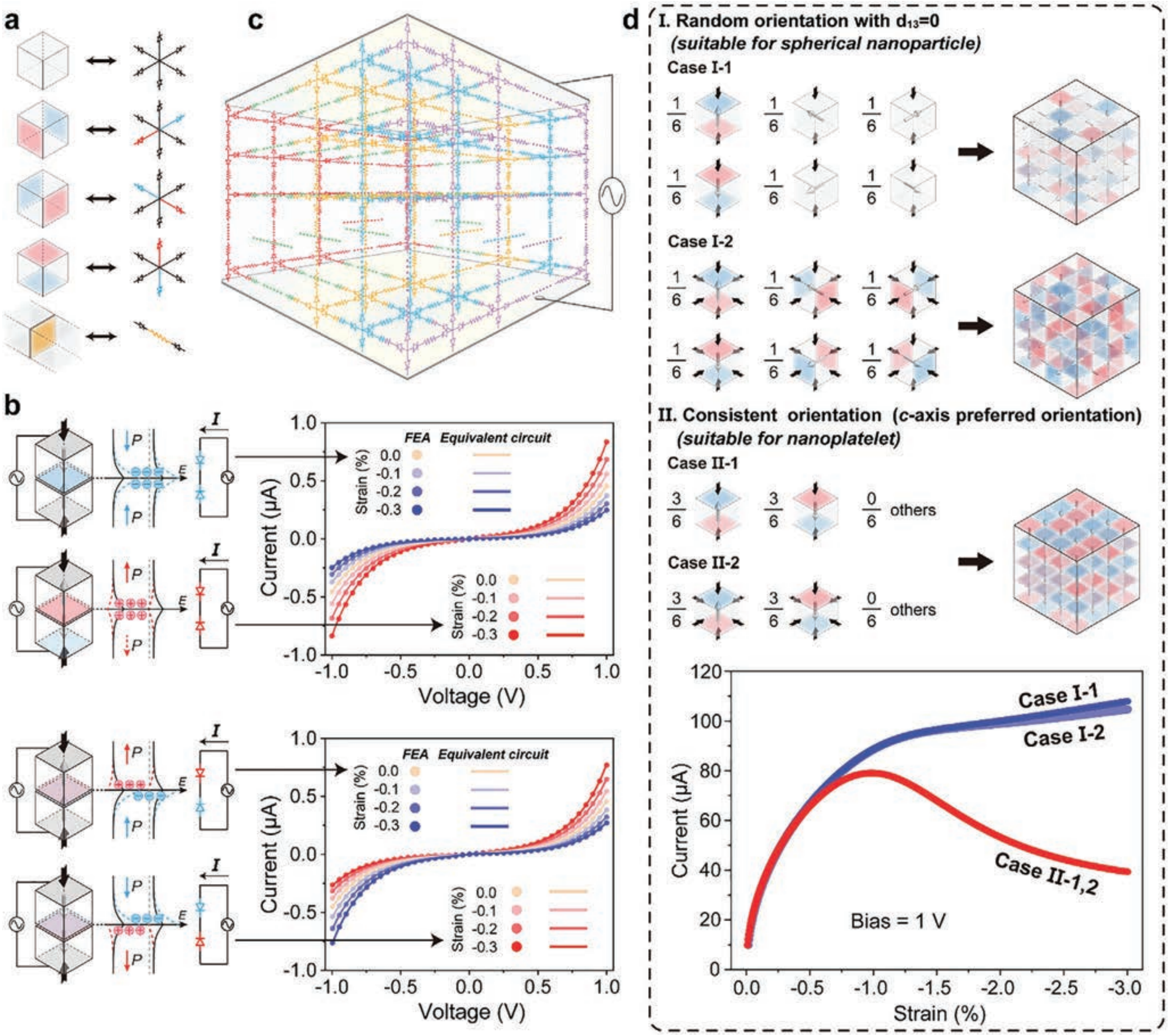

Figure 3. Simulation of statistical piezotronic effect. a) Schematic diagrams of the simplified piezoelectric units, contact resistance between them, and the corresponding equivalent circuits. Each piezoelectric unit is equivalent to a combination of six diodes. The red and blue diodes represent the interface barriers regulated by positive and negative piezoelectric potentials, respectively. The yellow resistance represents the contact resistance. b) Calculated *I–V* characteristics of typical interface "IV," "V," and "VI" in Figure 1c as a function of compressive strain by methods of "Finite Element Analysis" (color points) and corresponding equivalent circuits (color lines). The consistency of the two simulation results shows the possibility of using equivalent circuits to replace piezoelectric units. c) 3D equivalent circuit diagram of a bulk consisting $10 \times 10 \times 10$ piezoelectric units. d) Calculated statistical piezotronic modification of the current-strain of $10 \times 10 \times 10$ units with different orientation distribution (Case I-1, 2 and Case II-1, 2) by the method of "Electronics Design Automation". Cases I and II respectively represent the piezoelectric units with distributions of random orientation (suitable for spherical nanoparticles in Figure 2) and consistent orientation (*c*-axis preferred orientation, suitable for nanoplatelets in Figures 4 and 5) under uniaxial pressure and isostatic pressure. Note: in the case of *c*-axis preferred orientation (002) (Case II-1, 2), the current of bulk eventually decreases with increased strain.

to a simple circuit system, which can be easily simulated by the method of "Electronics Design Automation" (EDA) that is widely used in the field of digital systematic design.

Figure 3c shows a 3D equivalent circuit constructed to mimic a ZnO bulk consisting of $10 \times 10 \times 10$ piezoelectric nanocrystals. Particularly, two cases are focused on here: ZnO nanocrystals with random orientation (Case I) and *c*-axis preferred orientation (Case II). The probabilities of each *c*-axis direction are presented in Figure 3d. There are six possible orientations in Case I, in which the possibilities are all 1/6. In contrast, the directions of *c*-axis in Case II are only up or down, and their probabilities are both 3/6. Both uniaxial pressure (Case I-1 and Case II-1) and isostatic pressure (Case I-2 and Case II-2) are also considered here. The current of such $10 \times 10 \times 10$ nanocrystals was calculated by EDA. No matter in Case I or Case II, the calculated conductivities both exhibit critical behavior as a function of strain, and show similar properties under a uniaxial pressure or an isostatic pressure. The simulation of Case I, in which the conductivity

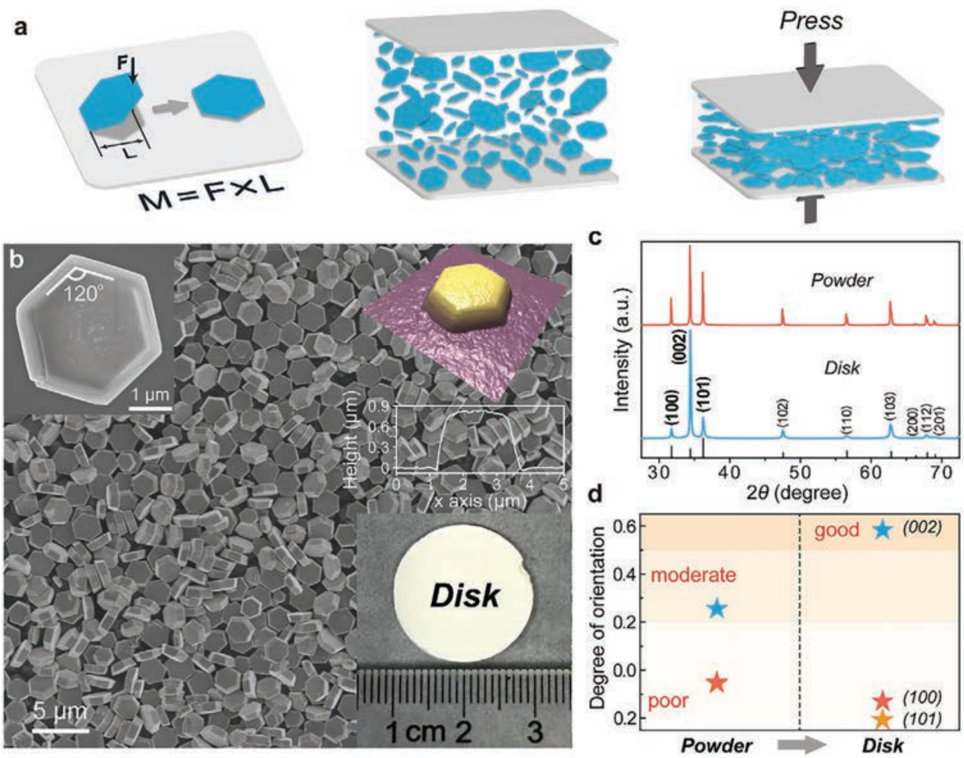

Figure 4. Statistical orientation degree of bulks made of ZnO nanoplatelets before and after pressing. a) Schematic diagram of nanoplatelet powder being pressed into bulk disk specimen, which can uniformly align the nanoplatelets in some degree by the torque induced by compressive force. b) SEM and AFM images of ZnO nanoplatelets, and the compressed disk made of ZnO nanoplatelets. c) XRD data of ZnO nanoplatelet powder and disk composed of ZnO nanoplatelets respectively. After pressing, the (002) diffraction intensity is obviously improved. d) Change of the statistical degree of orientation (Lotgering orientation factor) derived from the XRD data, indicating the greatly enhanced statistical orientation degree (good) of ZnO nanoplatelets after compressive pressing. The *c*-axis (002) is the preferred orientation.

increases with applied pressure, is consistent with the measured result of the bulk composed of ZnO spherical nanoparticles in Figure 2. While, it is important to note here that, compared with the bulk made of randomly oriented ZnO nanocrystals in Case I-1 and Case I-2, the conductivity of bulk containing *c*-axis preferred ZnO nanocrystal in Case II-1 and Case II-2 initially increases and eventually decreases with increasing strain. This simulation shows the possibility to control the conductivity of bulks composed of large interfaces under pressures by adjusting the distribution of nanocrystal orientation, which theoretically confirms our design scheme in Figure 1.

2.4. Bulks Made of ZnO Nanoplatelets

Next, we designed a scheme shown in **Figure 4**a to align the nanocrystals' orientation in bulks for effective piezotronic modulation. A torque generated by uniaxial compressive stress will align the plate-like nanocrystals in one direction.[14] ZnO nanoplatelets (Note S2 and Figure S2, Supporting Information) as shown in Figure 4b was synthesized through a low temperature hydrothermal method. It is a kind of piezoelectric nanocrystal (Figure S8, Supporting Information) with a standard hexahedral morphology and an aspect ratio of ≈0.4 (Figure S9, Supporting Information). The nanoplatelets were pressed into a disk-like bulk (inset of **Figure 5**b). X-ray diffraction spectrum was utilized to characterize the crystal orientation of powder and disk composed of ZnO nanoplatelets respectively. The enhanced peak (002) and suppressed peaks like (100) and (101), can be clearly observed from the change of X-ray diffraction spectra of the ZnO nanoplatelets powder before uniaxial compression and after uniaxial compression (Figure 4c), indicating the *c*-axis preferred orientation of ZnO nanoplatelets in the pressed disk (inset of Figure 4b). By calculating the Lotgering orientation factor *f*,[9] the degree of orientation is evaluated in Figure 4d. The (002) *c*-axis preferred orientation degree is more than two times enhanced after compression, accompanied with a decreased orientation degree of other directions. Therefore, the ZnO disk shows *c*-axis preferred orientation distribution of ZnO nanoplatelets.

2.5. Statistical Piezotronic Modification of ZnO Bulk Composed of *c*-Axis Preferentially Oriented ZnO Nanoplatelets

The statistical piezotronic modification of the electrical transport of the ZnO bulk disk composed of *c*-axis preferentially oriented ZnO nanoplatelets was studied. The *I–V* curves present a symmetrical Ohmic characteristic and the conductivity increases with decreasing external pressures from 483.1 to 163.5 MPa (Figure 5a), which is different from the previously ZnO bulk composed of randomly oriented ZnO nanoparticles

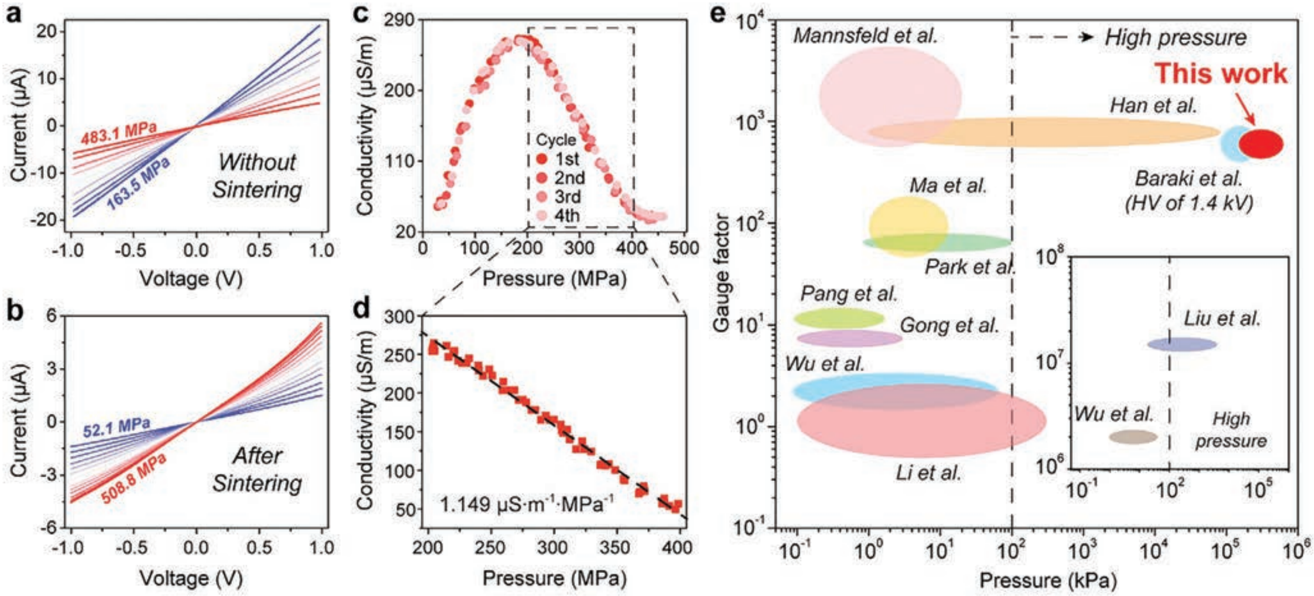

Figure 5. Statistical piezotronic modification of ZnO bulk composed of *c*-axis preferentially oriented ZnO nanoplatelets. a) *I*–*V* characteristics of the ZnO bulk without sintering under various pressures, indicating an increased current with decreased pressure. b) *I*–*V* characteristics of the ZnO bulk disk in a) after sintering under pressures. c) Variation of conductivity of the bulk without sintering. d) Enlarged details of the dotted box in (c), indicating a linear relationship between the conductivity and the applied pressure. e) Comparison of the gauge factor of this work with some existing piezotronic and piezoresistive sensors. “HV” represents “high voltage.”

in Figure 2. This comparison shows that the electrical control of the bulks is related to the statistical distribution of the crystals' *c*-axis orientation in bulks, indicating the dominant role of the piezotronic effect, rather than the piezoresistive effect. This trend of piezotronic regulation, making current to increase with decreasing pressure, is a particular phenomenon that occurs only in systems with a few interfaces and has not been observed previously in bulks with millions of interfaces. Further data analysis shows that the currents under biases of +1 V and −1 V both exhibit approximately linear relationship with applied pressures (Figure S10, Supporting Information). The linear regulation is also different from the piezotronic exponential regulation of a single interface or few interfaces. It may come from the statistical result of large numbers of interface regulations, showing the features of statistical piezotronic effect. The electrical transport of the ZnO bulk composed of *c*-axis preferentially oriented ZnO nanoplatelets after sintering was studied (Figure 5b), showing that current increases with increased pressures. It is opposite to the observed statistical piezotronic modulation of the ZnO bulk without sintering, but consistent with the results of the bulk composed of randomly oriented ZnO nanoparticles in Figure 2. During the sintering process, the crystal structure of ZnO nanoplatelets have been destroyed, resulting in randomly oriented ZnO nanocrystals (Figure S11, Supporting Information). Thus, the statistical piezotronic modulation becomes invalid in the ZnO bulk after sintering. This change further confirms the dominant regulation of the statistical piezotronic effect in the bulk of Figure 5a.

Additionally, the conductivity of the bulk (without sintering) consists of ZnO nanoplatelets with *c*-axis preferred orientation was further investigated (Figure 5c). As decreasing the pressure from 450 to 20 MPa, the conductivity initially increases to a maximum value at a pressure of ≈200 MPa, then begins to decrease, which coincides with the previous prediction using “Electronics Design Automation” in Figure 3d. As a comparison, apart from the randomly oriented ZnO spherical nanoparticles in Figure 2, we also measured the conductivities of non-piezoelectric materials such as TiO_2, BN, $ZnCO_3$ and $MgSO_4$ as under compressive pressures (Figure S12, Supporting Information), in which the conductivities gradually increase with increasing pressures. It mainly results from the strain-controlled contact potential/resistance, which is decreased with increasing pressures (Note S5 and Figures S5 and S6, Supporting Information). These comparison experiments further confirm that the electrical regulation of the bulk made of *c*-axis preferred ZnO nanoplatelets actually comes from piezotronic effect. Meanwhile, the consistency of the four cycles (Figure 5c) also indicates the modulation is reversible and reproducible. Particularly, as presented in Figure 5d, the conductivity exhibits a strong linear relationship with compressive pressures ranged from 200 and 400 MPa, which is consistent with the result of the inset of Figure 5a. A high sensitivity of 1.149 μS m^{-1} MPa^{-1} s and a corresponding gauge factor (defined as $[\Delta\sigma/\sigma(\varepsilon_{\text{low}})]/\Delta\varepsilon$) of 467–589 are obtained at the range of 200–400 MPa. Nevertheless, when the pressure exceeds ≈400 MPa, the increased barriers become large enough and hence will be difficult to further change the current channel, making the curve gradually becomes flattened.

As summarized in Figure 5e [15] and Table S2 (Supporting Information), the performance of ZnO bulk composed of preferentially orientated ZnO nanoplatelets as a static pressure sensor shows a high gauge factor particularly at the high-pressure range of 200–400 MPa, which exhibits the potential in high pressure sensing. Although various sensors with high gauge factor can achieve ultra-sensitive strain/stress sensing, they are usually flexible and mainly work at low pressure (usually from ≈Pa to ≈KPa). Most sensors are difficult to withstand such a high pressure, except for certain devices based on ceramic or single crystal bulk materials. Nevertheless, the main principle of these high-pressure sensors is the piezoelectric effect or piezoresistive effect. For some piezoelectric sensors based on bulk materials, they can work under high pressure but usually needs high frequency (≈kHz) and complicated structures (such as the novel POSFET, piezoelectric oxide semiconductor field effect transistor), thus limiting its application performance.[16] As for piezoresistive sensor, the high sensitivity is usually achieved at lower pressure range; while the performance under high pressure is very limited with gauge factor usually on the order of 100.[17] In contrast, the piezotronic sensor can perfectly achieve high gauge factor at high pressure range, but currently the controllable regulation is limited to the device containing only a few interfaces. The statistical piezotronic effect proposed here provides a controllable strategy to extend the piezotronic effect from nanoscale to macroscale, expanding its scope of practical applications. It is also worth noting that, although ZnO nanoplatelets are used here, it is equally feasible for other piezoelectric semiconductors in principle. Therefore, the statistical piezoelectric effect has wide potential in the field of high-pressure sensing.

3. Conclusion

In summary, a kind of statistical piezotronic effect is proposed and demonstrated to control a complex system through the preferred orientation of ZnO nanoplatelets. Unlike the regulation for a limited number of interfaces, the statistical piezotronic effect is a statistical phenomenon that the electrical transport of bulks containing large numbers of interfaces can be effectively modulated by controlling the orientation distributions of the nanocrystals and thus the interfacial piezo-potentials. A maximum sensitivity of 1.149 μS m^{-1} MPa^{-1} and a corresponding gauge factor of 467–589 at a high-pressure range of 200–400 MPa are obtained in the bulk with optimum preferred orientation of ZnO nanoplatelets. The statistical piezotronic effect can be used for macroscopic practical applications in tunable electronics and smart sensors.

Supporting Information

Supporting Information is available from the Wiley Online Library or from the author.

Acknowledgements

S.H.L. and H.M. contributed equally to this work. This research was supported by the National Key R&D Project from Minister of Science and Technology (2016YFA0202704), National Natural Science Foundation of China (No. 51472111, 51432005, 5151101243 and 51561145021), the Natural Science Basic Research Plan in Shaanxi Province of China (2019JQ-652), and the National Program for Support of Top-notch Young Professionals. The authors also thank Chupeng Yi for help with the simulations of equivalent circuits, and Zheng Wang for help with the fabrication of devices.

Conflict of Interest

The authors declare no conflict of interest.

Data Availability Statement

Research data are not shared.

Keywords

mechanical gating, piezoelectric effect, piezotronic effect, statistical distribution, ZnO nanoplatelets

Received: December 1, 2020
Revised: January 12, 2021
Published online:

[1] H. Kroemer, *Rev. Mod. Phys.* **2001**, *73*, 783.
[2] C.-H. Lee, G.-H. Lee, A. M. Van Der Zande, W. Chen, Y. Li, M. Han, X. Cui, G. Arefe, C. Nuckolls, T. F. Heinz, *Nat. Nanotechnol.* **2014**, *9*, 676.
[3] O. Lopez-Sanchez, D. Lembke, M. Kayci, A. Radenovic, A. Kis, *Nat. Nanotechnol.* **2013**, *8*, 497.
[4] a) W. Wu, L. Wang, Y. Li, F. Zhang, L. Lin, S. Niu, D. Chenet, X. Zhang, Y. Hao, T. F. Heinz, J. Hone, Z. L. Wang, *Nature* **2014**, *514*, 470; b) M. Si, A. K. Saha, S. Gao, G. Qiu, J. Qin, Y. Duan, J. Jian, C. Niu, H. Wang, W. Wu, S. K. Gupta, P. D. Ye, *Nat. Electron.* **2019**, *2*, 580; c) F. Zhang, P. Lv, Y. Zhang, S. Huang, C.-M. Wong, H.-M. Yau, X. Chen, Z. Wen, X. Jiang, C. Zeng, J. Hong, J.-Y. Dai, *Phys. Rev. Lett.* **2019**, *122*, 257601; d) L. Wang, S. Liu, X. Feng, C. Zhang, L. Zhu, J. Zhai, Y. Qin, Z. L. Wang, *Nat. Nanotechnol.* **2020**, *15*, 661.
[5] a) W. Wu, Z. L. Wang, *Nat. Rev. Mater.* **2016**, *1*, 116031; b) C. Pan, J. Zhai, Z. L. Wang, *Chem. Rev.* **2019**, *119*, 9303; c) Y. Yu, X. Wang, *Adv. Mater.* **2018**, *30*, 1800154.
[6] a) C. Pan, L. Dong, G. Zhu, S. Niu, R. Yu, Q. Yang, Y. Liu, Z. L. Wang, *Nat. Photonics* **2013**, *7*, 752; b) A. A. Shevyrin, A. G. Pogosov, A. K. Bakarov, A. A. Shklyaev, *Phys. Rev. Lett.* **2016**, *117*, 017702; c) P. Keil, M. Trapp, N. Novak, T. Frömling, H.-J. Kleebe, J. Rödel, *Adv. Mater.* **2018**, *30*, 1705573; d) H. Yuan, T. Lei, Y. Qin, R. Yang, *Nano Energy* **2019**, *59*, 84; e) S. Zhang, B. Ma, X. Zhou, Q. Hua, J. Gong, T. Liu, X. Cui, J. Zhu, W. Guo, L. Jing, *Nat. Commun.* **2020**, *11*, 1
[7] a) J. Qi, Y.-W. Lan, A. Z. Stieg, J.-H. Chen, Y.-L. Zhong, L.-J. Li, C.-D. Chen, Y. Zhang, K. L. Wang, *Nat. Commun.* **2015**, *6*, 7430; b) X. Wang, R. Yu, C. Jiang, W. Hu, W. Wu, Y. Ding, W. Peng, S. Li, Z. L. Wang, *Adv. Mater.* **2016**, *28*, 7234; c) S. Liu, L. Wang, Z. Wang, Y. Cai, X. Feng, Y. Qin, Z. L. Wang, *ACS Nano* **2018**, *12*, 1732; d) F. Xue, J. Zhang, W. Hu, W.-T. Hsu, A. Han, S.-F. Leung, J.-K. Huang, Y. Wan, S. Liu, J. Zhang, J.-H. He, W.-H. Chang, Z. L. Wang, X. Zhang, L.-J. Li, *ACS Nano* **2018**, *12*, 4976; e) S. Liu, L. Wang, X. Feng, J. Liu, Y. Qin, Z. L. Wang, *Adv. Mater.* **2019**, *31*, 1905436; f) K. Song, R. Zhao, Z. L. Wang, Y. Yang, *Adv. Mater.* **2019**, *31*, 1902831; g) L. Wang, S. Liu, Z. Zhang, X. Feng, L. Zhu, H. Guo, W. Ding, L. Chen, Y. Qin, Z. L. Wang, *Nano Energy* **2019**, *60*, 724.
[8] a) N. Raidl, P. Supancic, R. Danzer, M. Hofstaetter, *Adv. Mater.* **2015**, *27*, 2031; b) P. R. Emtage, *J. Appl. Phys.* **1977**, *48*, 4372.
[9] F. Lotgering, *J. Inorg. Nucl. Chem.* **1959**, *9*, 113.
[10] Y. Zhang, Y. Liu, Z. L. Wang, *Adv. Mater.* **2011**, *23*, 3004
[11] R. Baraki, N. Novak, M. Hofstaetter, P. Supancic, J. Roedel, T. Froemling, *J. Appl. Phys.* **2015**, *118*, 085703.
[12] a) Z. L. Wang, X. Kong, J.-M. Zuo, *Phys. Rev. Lett.* **2003**, *91*, 185502; b) H. B. Michaelson, *IBM J. Res. Dev.* **1978**, *22*, 72.

[13] A. C. Fischer-Cripps, *Introduction to Contact Mechanics*, Springer, New York **2007**.

[14] L. D. Landau, E. Lifshitz, Course of Theoretical Physics Vol. 7: Theory of Elasticity, Pergamon Press, Oxford **1986**.

[15] a) S. C. Mannsfeld, B. C. Tee, R. M. Stoltenberg, C. V. H. Chen, S. Barman, B. V. Muir, A. N. Sokolov, C. Reese, Z. Bao, *Nat. Mater.* **2010**, *9*, 859; b) C. Pang, G.-Y. Lee, T.-i. Kim, S. M. Kim, H. N. Kim, S.-H. Ahn, K.-Y. Suh, *Nat. Mater.* **2012**, *11*, 795; c) W. Wu, X. Wen, Z. L. Wang, *Science* **2013**, *340*, 952; d) R. Baraki, N. Novak, T. Froemling, T. Granzow, J. Roedel, *Appl. Phys. Lett.* **2014**, *105*, 111604; e) S. Gong, W. Schwalb, Y. Wang, Y. Chen, Y. Tang, J. Si, B. Shirinzadeh, W. Cheng, *Nat. Commun.* **2014**, *5*, 3132; f) X. Han, W. Du, R. Yu, C. Pan, Z. L. Wang, *Adv. Mater.* **2015**, *27*, 7963; g) Y. Li, S. Luo, M. C. Yang, R. Liang, C. Zeng, *Adv. Funct. Mater.* **2016**, *26*, 2900; h) M. Park, Y. J. Park, X. Chen, Y. K. Park, M. S. Kim, J. H. Ahn, *Adv. Mater.* **2016**, *28*, 2556; i) X. Wu, Y. Han, X. Zhang, Z. Zhou, C. Lu, *Adv. Funct. Mater.* **2016**, *26*, 6246; j) S. Liu, L. Wang, X. Feng, Z. Wang, Q. Xu, S. Bai, Y. Qin, Z. L. Wang, *Adv. Mater.* **2017**, *29*, 16063461606346; k) Y. Ma, N. Liu, L. Li, X. Hu, Z. Zou, J. Wang, S. Luo, Y. Gao, *Nat. Commun.* **2017**, *8*, 1207.

[16] R. S. Dahiya, M. Valle, *Robotic Tactile Sensing: Technologies and System*, Springer Science & Business Media, Dordrecht **2013**.

[17] C. Liu, *Foundations of MEMS*, Pearson Education, Inc., Upper Saddle River, New Jersey **2012**.

